Journal of Luminescence 129 (2009) 1786–1789

Contents lists available at ScienceDirect

Journal of Luminescence

journal homepage: www.elsevier.com/locate/jlumin

Study of luminescent defects in hafnia thin films made with different deposition techniques

Alessandra Ciapponi, Frank R. Wagner *, Stéphanie Palmier, Jean-Yves Natoli, Laurent Gallais

Institut Fresnel, CNRS, Aix-Marseille Université, Ecole Centrale Marseille, Campus de Saint-Jérôme, 13013 Marseille, France

ARTICLE INFO

Available online 2 April 2009

PACS:
78.55._m
78.67.Bf
61.80.Ba

Keywords:
HfO_2
Thin film
Optical applications
Laser damage
Luminescence
Crystallinity

ABSTRACT

Hafnia thin films for high-power optical coatings have been characterized by photoluminescence pumped by 4.66 eV photons and photothermal deflection measurements. These data are compared to the statistical laser damage behavior in order to find correlations between destructive and non-destructive characterizations. Thin films have been produced at two thicknesses and using different thin-film deposition techniques typically employed for optical coating fabrication: EBD (HfO_2 target), EBD (Hf target), RLVIP and DIBS. The photoluminescence spectra show significant differences depending on the deposition techniques and thicknesses. EBD films show significant luminescence but the luminescence of ion-assisted films could not be distinguished from the uncoated substrate. All EBD coating spectra could be described by a linear combination of four bands. Further, XRD measurements show that the 255-nm-thick films had a relatively high crystallinity: EBD films contained the monoclinic phase and the ion-assisted films contained oriented nanocrystals of orthorhombic hafnia. The presence of orthorhombic phases indicates high compressive strain quenching the photoluminescence of these samples.

1. Introduction

In the domain of high-power photonics, laser-induced damage of optical components is an important limitation for the development of optical systems. Compact and powerful laser systems are limited in their specifications or their lifetime by laser-induced damage. Generally, laser-induced damage occurs on surfaces or optical multilayer coatings like mirrors and anti-reflection coatings [1]. The widely accepted model for the initiation of laser damage in the nanosecond regime considers the presence of nanometer-sized precursor defects in the tested materials. The main reason to think that laser-induced damage is precursor mediated is the fact that laser damage appears at electric field strengths that are at least a factor of ten too weak to generate avalanche ionization [2]. The probability of encounter between the high-power region of the laser beam and a damage precursor will determine the damage probability at a certain energy density or "fluence".

Destructive techniques enable us to evaluate a material statistically by the measurement of the laser damage probability as a function of fluence. Besides the determination of the damage threshold, these techniques may also provide information on the number of different damage precursors in the material and their respective volume densities [3]. However, it is difficult to conclude on the physical and chemical nature of the damage precursors based on destructive measurements only.

Non-destructive analyzing methods like highly sensitive photothermal deflection measurements (PTM) or photoluminescence (PL) would be highly appreciated if it was possible to find a correlation with destructive laser-damage data. We present a non-destructive investigation on hafnia monolayers as they are frequently used as high index material for the fabrication of optical multilayer's aiming high-power applications [4,5].

2. Samples and deposition techniques

Hafnia monolayers of two thicknesses have been deposited on synthetic-fused silica substrates. Substrates have been provided with a high-power polish and have been cleaned simultaneously by an optimized procedure. Four deposition techniques typical for optical coating fabrication have been employed: electron beam deposition using a metallic hafnium target in an oxygen partial pressure (EBD-Hf), electron beam deposition using a hafnia target in the same atmosphere (EBD-HfO_2), reactive low-voltage ion plating (RLVIP) and dual ion beam sputtering (DIBS). EBD with either target results in porous coatings with refractive indices lower than the bulk refractive index of HfO_2. RLVIP and DIBS are ion-assisted techniques that yield dense coatings with higher refractive index. More details on the deposition parameters can be found in an earlier paper [6].

* Corresponding author. Tel.: +33 4 91 28 83 93; fax: +33 4 91 28 80 67.
E-mail address: frank.wagner@fresnel.fr (F.R. Wagner).

0022-2313/$ - see front matter © 2009 Elsevier B.V. All rights reserved.
doi:10.1016/j.jlumin.2009.02.026

3. Destructive characterization

The thickness of the samples has been chosen to minimize the influence of the electrical field distribution during the destructive laser damage tests [7]. All samples were "2H" at the test wavelength. This corresponds to a physical thickness of approximately 255 nm for the layers intended for infrared usage ($\lambda = 1064$ nm) and approximately 85 nm for the layers intended for ultraviolet usage ($\lambda = 355$ nm). Thus the thick layers are about three times thicker as the thin layers.

Destructive laser damage tests have been realized using a standard 1-on-1 laser damage test [8]. Briefly, this means that the laser damage probability, P, at a given fluence, F, has been determined by irradiating, N, isolated sites with one laser pulse each. With k damaged sites, the damage probability for the tested fluence is $P(F) = k/N$. Distinct differences have been found in the laser damage probability curves $P(F)$ for the different samples, all representing the same optical function. The laser damage thresholds in the UV (355 nm, 12 ns pulse duration) are 18, 2.1, 2.8, 2.3 and 0.2 J/cm^2 for the uncoated substrate, the EBD-HfO_2 sample, the EBD-Hf sample, the RLVIP sample and the DIBS sample, respectively. A more detailed description of these results can be found in Ref. [6].

4. Non-destructive characterization

4.1. Averaged photothermal deflection measurements

Averaged photothermal measurements have been carried out at 351 nm wavelength in order to check for possible correlations between laser damage performance at 355 nm and the measured absorption. The used photothermal deflection measurement setup has been described in detail in Ref. [9]. Briefly, a continuous wave argon-ion laser at 351 nm wavelength is focused onto the sample. A He–Ne probe beam is focused close to the focus of the pump beam forming an angle of about 30° with the pump beam. The absorption of the pump beam in the sample causes periodic heating and cooling of the focal volume. The probe beam is deflected due to the reactive index change induced by the heating of the pumped volume (mirage effect). The probe beam deflection is sensed by a four-quadrant photodiode and the corresponding deflection signal is amplified using a lock-in amplifier [10].

The setup has been calibrated using a specially developed Ti-ion implanted silica samples with known absorption (measured by photo-spectrometry). For the detailed calibration procedure allowing us to perform absolute absorption measurements with PTM, please refer to Ref. [9]. The measured values for the imaginary part of the refractive index are 2.9×10^{-4}, 8.7×10^{-5}, 1.7×10^{-4} and 2.7×10^{-3} for the EBD-HfO_2 sample, the EBD-Hf sample, the RLVIP sample and the DIBS sample, respectively.

Comparison of laser damage thresholds at 355 nm wavelength and the extinction coefficients at 351 nm wavelength show a clear correlation between strong absorption and low damage threshold. This result indicates that the improved mechanical and thermal properties of the dense DIBS films are overbalanced by the more important energy deposition due to the higher absorption.

4.2. Thin-film homogeneity by PL and PTM

Spatially averaged absorption measurements only allow finding correlations with destructive damage data if the absorption level is rather high. For better-quality coatings a spatially resolved approach can provide more interesting data as has been shown in recent studies on model materials like silica with embedded gold nanoparticles [11]. Furthermore, we will show in this section that different kinds of defects may be identified using simultaneous mapping of photothermal deflection, wavelength-integrated luminescence and the scattering signal.

Fig. 1 shows an example for these simultaneous mappings that indicate the existence of different defect types in the optical thin films. Three different defects are labeled by D_1, D_2 and D_3.

Defect D_1 shows scattering and luminescence signal only and is most likely a kind of surface contamination by a luminescent particle. Defect D_2 shows scattering and absorption signal only and may thus be classified as surface contamination too, but the particle is of a different type as no luminescence is observed. Finally, defect D_3 is only visible in the luminescence map. As the luminescent defect is embedded in the thin film it is most likely to cause damage upon high-power irradiation.

A zoom on defect D_3 shows that there is, as expected, a weak absorption signal too (not shown). These mappings have been done with a relatively large pump beam (diameter 30 μm), which limits the spatial resolution of the maps. Defect D_3 may thus better be regarded as an assembly of several non-resolved defects.

Theoretically, we may improve the spatial resolution of the measurement up to the diffraction limit; however, the geometry of our setup does not allow very short focal distances for the focusing objective of the pump beam. Nevertheless using a diameter of 3 μm we are already able to separate smaller luminescent defects and thus approach the relevant laser damage precursors. Fig. 2 shows the high-resolution luminescence mapping.

We see that the average luminescence of the sample is generated by many small but strongly luminescent defects. For comparison, Fig. 3 shows a microscope image of a zone on the same sample as Fig. 2. The area included in the dashed ellipse has been irradiated with fluence close to the damage threshold. The precursor-mediated damage initiation is confirmed by the morphology of the damage and the density of damage precursors

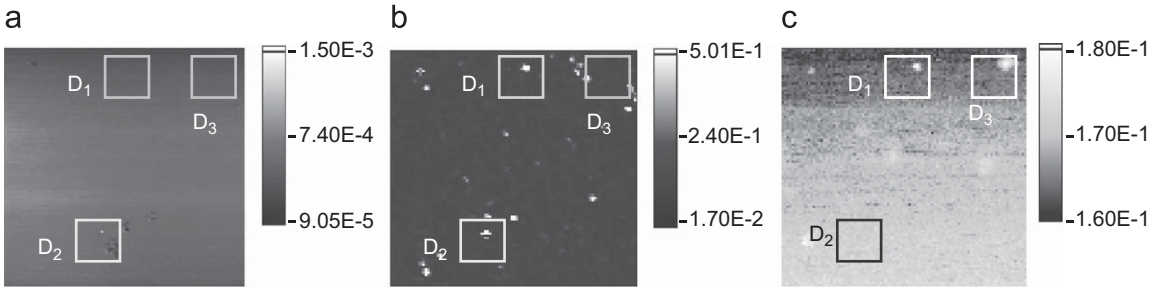

Fig. 1. Photothermal absorption (a), scattering (b) and luminescence (c) maps in arbitrary units acquired simultaneously on a 1.5 mm × 1.5 mm zone of the sample (DIBS, thickness 85 nm). The 351 nm pump beam was focused to a diameter of 30 μm.

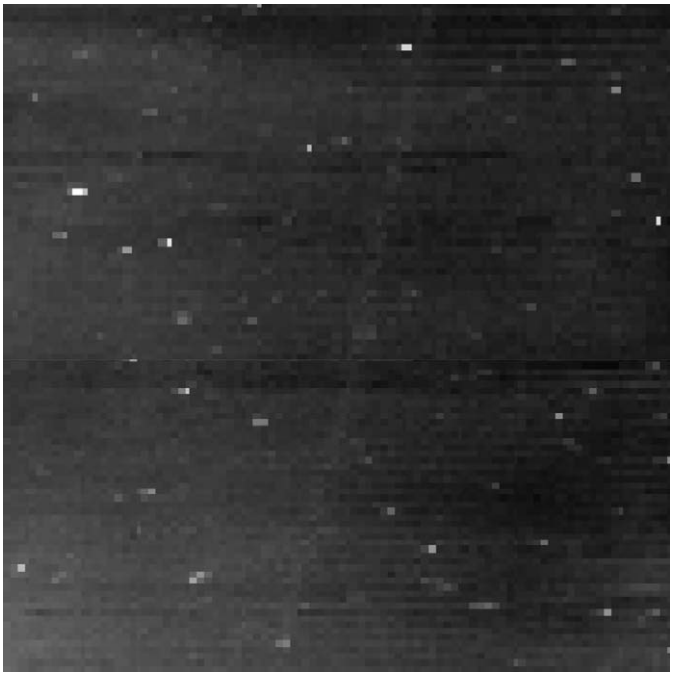

Fig. 2. High-resolution luminescence mapping of the RLVIP sample. Several small luminescent defects can be distinguished.

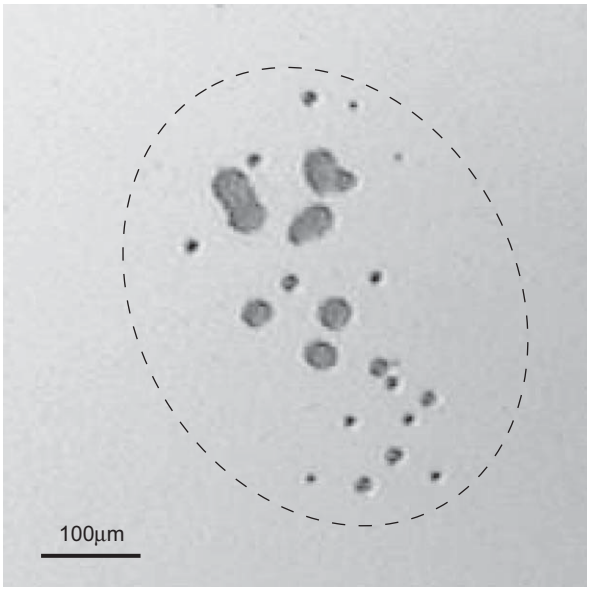

Fig. 3. Optical micrograph of laser-induced damage in a hafnia film deposited by RLVIP. The sample has been irradiated at fluence slightly above the damage threshold. The damage morphology shows the importance of defects for the damage initiation.

is of the same order of magnitude as the density of the luminescent defects in Fig. 2.

More efforts will be necessary in the future to further approach the detection of a single laser damage precursor by these methods, but it is clear that the luminescence signal contains unique information on the observed defects.

4.3. Photoluminescence spectra

Spectrally resolved photoluminescence measurements at room temperature have been performed on all samples. The pump source is the forth harmonic of a Q-switched Nd:YAG laser at 266 nm (4.66 eV). The pulse duration (FWHM) of the pulses is 10 ns and the applied fluence was approximately 2 mJ/cm^2. Diffused pump light, as well as the remaining second harmonic of the pump laser at 532 nm, has been rejected by a notch filter. The acquisition of a spectrum accumulated 2000 laser pulses and the obtained spectra are thus time averaged. The presented spectra have been corrected for the instrument response (notch filter, collection optics, fiber, monochromator and detector) using a calibrated light source. The spectrometer is made up by a Czerny–Turner imaging monochromator ($f = 300$ mm, Acton SpectraPro 2300i) coupled to a bundle of optical fibers and an intensified CCD camera (Princeton Instruments PI-MAX system). Spatial averaging of the luminescence over the entire pumped area has been performed by placing the fiber bundle in the focal plane of the UV-grade fused silica lens used to collect the luminescence light.

Fig. 4 shows the obtained luminescence spectra for thin and thick samples deposited with different deposition techniques and, for reference, the signal obtained from an uncoated substrate. The data influenced by the presence of the 532 nm notch filter has been removed. The most striking feature of Fig. 4 is that the luminescence intensity depends less on the thickness of the sample than on the deposition technique. The EBD samples show relatively strong luminescence whereas the luminescence levels of the RLVIP and DIBS samples are similar to the luminescence of the uncoated substrate.

Searching for reports on luminescence of hafnia coatings in literature yields mainly four publications [12–15] all of them being motivated by microelectronics applications, where HfO_2 is a potential high-k oxide for transistor gates. In consequence, the investigated deposition techniques are mainly atomic layer deposition (ALD) [12,14] and chemical vapor deposition (CVD) [13,15]. However, pulsed laser deposition (PLD) has also been used [13]. All authors pumped the photoluminescence with photon energies of at least 5.8 eV as compared to our pump source at 4.66 eV. The lower pump photon energy in our study is most probably the reason why the exciton-related peak at 4.4 eV is

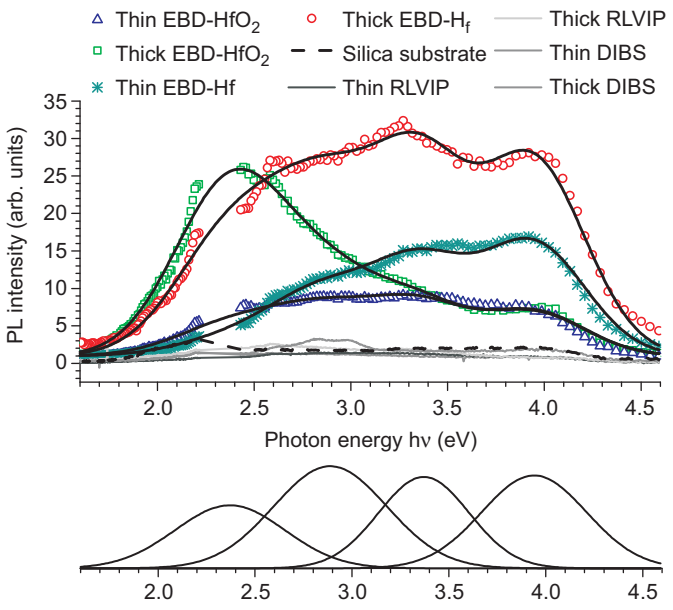

Fig. 4. Photoluminescence spectra of hafnia coatings and of an uncoated substrate (thick dashed line). The solid black lines are linear combinations of the Gaussian peaks shown under the experimental data. Peak positions and FWHM widths after fitting are: 2.4/0.65, 2.9/0.68, 3.4/0.55 and 3.95/0.63 eV from the left to the right.

missing in our spectra [12,14]. In this study, we only see defect-related luminescence that might be important for the understanding of laser-induced damage in these coatings.

In the following, we will concentrate on the spectra of EBD samples as in these cases the luminescence clearly comes from the hafnia coating. The EBD spectra show the presence of similar spectral components for both thicknesses and target types, the most evident being a component close to 4.0 eV. However, in contrast to the findings of Ito et al. [14], we see clear differences between the shapes of the luminescence spectra corresponding to different target types and different thicknesses. Compiling the literature reports and comparing them with our data we find four bands centered at about: 4.0, 3.4, 2.8 and 2.4 eV, respectively [12–15].

Simultaneous fitting of the EBD luminescence spectra with Gaussian peaks centered at these positions yield the solid black lines presented in Fig. 4.

For complementary information, we also performed X-ray diffraction measurements on all samples. The 255-nm-thick samples showed a partially crystalline structure for all tested deposition techniques. The XRD data have been acquired with a Philips Xpert MPD diffractometer (Xcelerateur detector). The crystalline phase of both thick EBD samples was identical and could be identified as randomly oriented crystals of monoclinic HfO_2 [16]. The crystallinity of the ion-assisted samples however (RLVIP and DIBS), was oriented and orthorhombic [17]. In fact, the orthorhombic phases of HfO_2 are the high-pressure phases of this material [18,19] and their presence thus indicates high compressive strain in these layers. This confirms the conclusions derived from the mechanical properties of ion-assisted thin films. Then, during the luminescence measurements the high compressive strain quenches the photoluminescence of these hafnia layers.

The XRD measurements further show that only the thin films deposited by EBD-Hf are homogeneous. In all other thin samples, the X-ray diffraction peaks practically disappear indicating amorphous coatings for the 85-nm-thick samples. For the EBD-Hf samples the diffraction peaks scale with film thickness.

Due to the homogeneity of EBD-Hf thin films and the fact that we measured luminescence spectra for two samples of different thickness, we can isolate the volume contribution and the interface contribution to the luminescence spectra using a very simple model: as the thickness ratio between the thick and the thin samples equals three, the volume contribution will be three times more important for the thick films compared to the thin ones. Neglecting reabsorption of the emitted luminescence, the same interface contribution adds to the volume contribution. We may express this by two linear equations that are valid for the luminescence signal at all wavelengths: *thin* = *interface*+*volume* and *thick* = *interface*+3**volume*. Eliminating the interface contribution we may thus deduce the contribution of the film volume only: *volume* = (*thick*−*thin*)/2. Fig. 5 compares the contribution of the film volume only to the luminescence spectrum of the thin sample.

We may conclude from Fig. 5 that the luminescence spectra contain an important interface contribution which is limited to the high-energy peaks of the spectra.

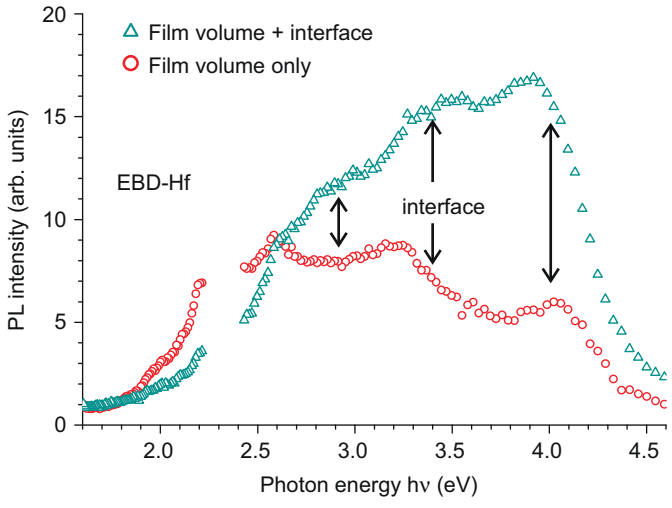

Fig. 5. Photoluminescence spectrum of the thin EBD-Hf sample (triangles) and the volume contribution of the hafnia thin film to the luminescence spectrum (circles).

5. Summary and conclusion

We showed that luminescence studies add complementary information to absorption and scattering data. Absorption, scattering and luminescence maps recorded with high sensitivity and high spatial resolution allow to distinguish different types of defects on optical thin films. Films made by different deposition techniques can be distinguished by their luminescence spectra. XRD measurements show that ion-assisted deposition techniques create high compressive strain in thin films, which in turn quenches the luminescence. For one deposition technique (EBD-Hf), XRD data showed that the films are homogeneous and in consequence we could separate the contributions of the interface and the film volume on the luminescence signal.

In summary, photoluminescence has shown to be a useful tool for non-destructive characterization of hafnia thin films for optical applications in view of laser damage testing of these films. More detailed studies are however necessary in order to establish a strong link between luminescence data and the laser damage threshold for this material.

Acknowledgements

We want to thank Carine Perrin-Pellegrino of the IM2NP for the XRD measurements and the RCMO group of the Institut Fresnel Marseille for the sample preparation.

References

[1] R.M. Wood, Laser-Induced Damage of Optical Materials, Institut of Physics Publishing, 2003.
[2] A.M. Rubenchik, M.D. Feit, SPIE 4679 (2002) 79.
[3] J.Y. Natoli, L. Gallais, H. Akhouayri, C. Amra, Appl. Opt. 41 (2002) 3156.
[4] A.K. Burnham, M. Runkel, M.D. Feit, A.M. Rubenchik, R.L. Floyd, T.A. Land, W.J. Siekhaus, R.A. Hawley-Fedder, Appl. Opt. 42 (2003) 5483.
[5] M. Alvisi, M. Di Giulio, S.G. Marrone, M.R. Perrone, M.L. Protopapa, A. Valentini, L. Vasanelli, Thin Solid Films 358 (2000) 250.
[6] B. Pinot, H. Leplan, F. Houbre, E. Lavastre, J.C. Poncetta, G. Chabassier, SPIE 4679 (2001) 235.
[7] L. Gallais, J. Capoulade, J.Y. Natoli, M. Commandre, M. Cathelinaud, C. Koc, M. Lequime, Appl. Opt. 47 (2008) C107.
[8] H. Krol, C. Amra, C. Grezes-Besset, M. Commandre, SPIE 6720 (2008) V7200.
[9] International Organization for Standardization, ISO 11254-1 (2000).
[10] L. Gallais, M. Commandre, Appl. Opt. 45 (2006) 1416.
[11] M. Commandre, P. Roche, Appl. Opt. 35 (1996) 5021.
[12] B. Bertussi, J.Y. Natoli, M. Commandre, J.L. Rullier, F. Bonneau, P. Combis, P. Bouchut, Opt. Commun. 254 (2005) 299.
[13] J. Aarik, H. Mändar, M. Kirm, L. Pung, Thin Solid Films 466 (2004) 41.
[14] T. Ito, M. Maeda, K. Nakamura, H. Kato, Y. Ohki, J. Appl. Phys. 97 (2005) 054104.
[15] M. Kirm, J. Aarik, M. Jurgens, I. Sildos, Nucl. Instrum. Methods Phys. Res. A 537 (2005) 251.
[16] A.A. Rastorguev, V.I. Belyi, T.P. Smirnova, L.V. Yakovkina, M.V. Zamoryanskaya, V.A. Gritsenko, H. Wong, Phys. Rev. B 76 (2007).
[17] Joint Committee of Powder Diffraction Standards, Card 43-1017.
[18] F.K. Inorganic Cryst. Structure Database, Collection Code 71354 (1999).
[19] J.M. Leger, A. Atouf, P.E. Tomaszewski, A.S. Pereira, Phys. Rev. B 48 (1993) 93.